

Journal on Scientific Computing, vol. 19, (2003), 293–308

The Computation of Martensitic Microstructure with
Piecewise Laminates

Martin Kružík
Center of Advanced European Studies And Research
Friedensplatz 16
D-53111 Bonn Germany

Mitchell Luskin
206 Church St. SE
School of Mathematics
University of Minnesota
Minneapolis, MN 55455
U.S.A.

Abstract

We present a numerical method for the approximation of microstructure in martensitic crystals by piecewise laminates, and we give computational results for several three-dimensional models of martensitic microstructure by using piecewise second-order laminates.

The computation of martensitic microstructure with piecewise laminates

Martin Kružík[†] Mitchell Luskin[‡]

submitted July 16, 2002, revised November 4, 2002

Dedicated to Stanley Osher on the occasion of his 60th birthday

1 Introduction

Martensitic crystals are observed in nature and technology to be in metastable states with a complex microstructure mixing the austenitic (high temperature) phase with multiple symmetry-related variants of the martensitic (low temperature) phase [5, 6, 26]. Defects and impurities created during the formation of the crystal can also influence both microscopic and macroscopic behavior.

During the past decade, numerical methods have been developed, analyzed, and utilized to investigate martensitic and magnetic microstructure at a range of length scales [8, 10–15, 18, 19, 21–29, 31]. In this paper, we explore a numerical approach that utilizes second-order laminates within piecewise linear finite elements to approximate martensitic microstructure. This method is motivated by an approximation theorem for the rank-one convexification [20] and by the approach of relaxation [16, 17, 24, 26, 32, 33]. The corresponding numerical approximation has been given for some two-dimensional problems in [21, 25, 31]. In this paper, we present compu-

*This work was supported in part by NSF DMS 95-05077, by NSF DMS-0074043, by AFOSR F49620-98-1-0433, by the Institute for Mathematics and Its Applications, by the Institute for Pure and Applied Mathematics, by the Minnesota Supercomputer Institute, and by GA AV ČR grant no. A 107 5005.

[†]Center of Advanced European Studies And Research, Friedensplatz 16, D-53111 Bonn Germany, and Institute of Information Theory and Automation, Academy of Sciences of the Czech Republic, Pod vodárenskou věží 4, CZ-182 08, Praha 8, Czech Republic. Email: kruzik@caesar.de, kruzik@utia.cas.cz.

[‡]206 Church St. SE, School of Mathematics, University of Minnesota, Minneapolis, MN 55455, U.S.A. Email: luskin@math.umn.edu.

tational results for several three-dimensional models of martensitic microstructure by using piecewise second-order laminates.

2 The geometrically nonlinear theory of martensite

The elastic energy of a martensitic crystal at a fixed temperature θ is modeled in the geometrically nonlinear theory [5, 6, 26] by

$$\int_{\Omega} W(\nabla u(x)) \, dx,$$

where $\Omega \subset \mathbb{R}^3$ is the reference domain of the crystal, $u : \Omega \rightarrow \mathbb{R}^3$ denotes the deformation, and $W : \mathbb{R}^{3 \times 3} \rightarrow \mathbb{R}$ is the frame-indifferent free energy density (with the fixed temperature not explicitly denoted).

At temperatures below the transformation temperature, θ_T , the energy density W has a multiple well structure in which there are M distinct matrices, F_1, \dots, F_M , $\det F_i > 0$, with the property (after normalization) that

$$W \geq 0 \quad \text{and} \quad W(F) = 0 \quad \text{if and only if} \quad F \in \bigcup_{i=1}^M \text{SO}(3)F_i,$$

where $\text{SO}(3)$ is the group of proper rotations. We assume that the wells $\text{SO}(3)F_i$ are distinct. If there exist $R_{ij} \in \text{SO}(3)$, $1 \leq i < j \leq M$, such that $\text{rank}(F_i - R_{ij}F_j) = 1$, then we say that W has *rank-one* connected wells. Figure 1 shows a cartoon for W for $M = 2$.

We also assume that the energy density $W(F)$ is continuous and satisfies the growth condition for large F given by

$$W(F) \geq C_1 \|F\|^p - C_0 \quad \text{for all } F \in \mathbb{R}^{3 \times 3}, \quad (2.1)$$

where $\|\cdot\|$ is a norm on $\mathbb{R}^{3 \times 3}$ and C_0 and C_1 are positive constants independent of $F \in \mathbb{R}^{3 \times 3}$. We also assume that $p > 3$ to ensure that deformations with finite energy are uniformly continuous. This growth condition (2.1) is convenient for the theoretical justification of the approximation, but it is not required for the utilization of the algorithm.

The bulk energy (up to an additive constant) of a martensitic crystal acted upon by a body force with density $f : \Omega \rightarrow \mathbb{R}^3$ can be modeled by

$$I(u) = \int_{\Omega} (W(\nabla u(x)) - f(x) \cdot u(x)) \, dx = \int_{\Omega} \Phi(x, u(x), \nabla u(x)) \, dx,$$

where for the sake of simplicity we have introduced

$$\Phi(x, u(x), \nabla u(x)) = W(\nabla u(x)) - f(x) \cdot u(x).$$

Metastable states of the crystal are characterized as local minima of the energy $I(u)$ with respect to the space of admissible deformations

$$\mathcal{A}_{u_0} = \{u \in W^{1,p}(\Omega; \mathbb{R}^3) : u = u_0 \text{ on } \Gamma, \det \nabla u > 0\},$$

where Γ is a non-empty, open subset of $\partial\Omega$ and $u_0 \in W^{1,p}(\Omega; \mathbb{R}^3)$ describes the boundary constraint. Although the notion of a local minimum is not uniquely defined for the continuous problem, the notion is well-defined for the finite-dimensional numerical approximations to be described in the following. We will motivate our numerical method by considering results for the minimization of the energy $I(u)$, although our methods more generally compute metastable states by numerical continuation of the loads and boundary constraints. The metastability of martensite has been explored for a thin film model by continuation in the loading in [7] and by nucleation in [9]. Recently, other models have been developed to treat the hysteresis in martensitic materials [1–4, 30, 35, 36].

3 The rank-one convexification and its approximations

A function $\tilde{\Phi} : \mathbb{R}^{3 \times 3} \rightarrow R$ is *rank-one convex* if

$$\tilde{\Phi}(\lambda A + (1 - \lambda)B) \leq \lambda \tilde{\Phi}(A) + (1 - \lambda)\tilde{\Phi}(B)$$

whenever $\text{rank}(A - B) \leq 1$ and $0 \leq \lambda \leq 1$. If a double well energy density has rank-one connected wells, one can easily see that it is not rank-one convex since it is clear from Figure 1 that W is not convex on the line segment $[F_1, F_2]$ with rank-one connected endpoints.

We can define the rank-one convex envelope $R\tilde{\Phi}$ of $\tilde{\Phi}$ by (see [16, Sec.1])

$$R\tilde{\Phi}(x, u, \cdot) = \sup\{\tilde{\Phi} \leq \tilde{\Phi}(x, u, \cdot) : \tilde{\Phi} \text{ rank-one convex}\}$$

for all $x \in \Omega$ and $u \in \mathbb{R}^3$, where we use standard function ordering to define $\tilde{\Phi} \leq \tilde{\Phi}(x, u, \cdot)$ to mean that

$$\tilde{\Phi}(F) \leq \tilde{\Phi}(x, u, F) \quad \text{for all } F \in \mathbb{R}^{3 \times 3}.$$

Using this envelope, we can consider the (local) minimization of the energy

$$I_R(u) = \int_{\Omega} R\tilde{\Phi}(x, u(x), \nabla u(x)) dx \quad \text{for } u \in \mathcal{A}_{u_0}. \quad (3.1)$$

The rank-one convex envelope is characterized by the following proposition.

Theorem 3.1 (see [16, 20]) Let $\tilde{\Phi} : \mathbb{R}^{3 \times 3} \rightarrow \mathbb{R}$ be bounded below. Then for every $A \in \mathbb{R}^{3 \times 3}$,

$$R\tilde{\Phi}(A) = \lim_{k \rightarrow \infty} R_k \tilde{\Phi}(A),$$

where $R_0 \tilde{\Phi} = \tilde{\Phi}$ and

$$R_{k+1} \tilde{\Phi}(A) = \inf \{ \lambda R_k \tilde{\Phi}(A_0) + (1 - \lambda) R_k \tilde{\Phi}(A_1) : 0 \leq \lambda \leq 1, \\ A = \lambda A_0 + (1 - \lambda) A_1, \text{rank}(A_1 - A_0) \leq 1 \}.$$

It follows directly from the definition that

$$\tilde{\Phi} \geq R_1 \tilde{\Phi} \geq \dots \geq R_k \tilde{\Phi} \geq R_{k+1} \tilde{\Phi} \geq \dots \geq R\tilde{\Phi}.$$

If $W(F_1) = W(F_2) = 0$ and $\text{rank}(F_1 - F_2) \leq 1$, then $RW(F) = 0$ for any $F \in \mathbb{R}^{3 \times 3}$ on the line segment with end points F_1 and F_2 . Thus, the dashed line on Figure 1 shows the rank-one convex envelope between rank-one connected gradients.

Utilizing this characterization of the rank-one convex envelope, we can consider the variational problem

$$\inf \{ I_k(u) : u \in \mathcal{A}_{u_0} \}, \quad (3.2)$$

where

$$I_k(u) = \int_{\Omega} R_k \Phi(x, u(x), \nabla u(x)) dx$$

and $R_k \Phi$ is the k^{th} order approximation of the rank-one convex envelope of Φ defined in Proposition 3.1. Of course, the minimum of I_k does not have to exist because $R_k \Phi$ is not necessarily quasiconvex [16]. On the other hand, we will see that finite element discrete solutions to (3.2) always exist and describe the martensitic microstructure observed in nature [26]. Due to the relaxation theorem [16], we have that

$$\begin{aligned} & \inf \left\{ \int_{\Omega} \Phi(x, u(x), \nabla u(x)) dx : u \in \mathcal{A}_{u_0} \right\} \\ &= \inf \left\{ \int_{\Omega} R_k \Phi(x, u(x), \nabla u(x)) dx : u \in \mathcal{A}_{u_0} \right\} \\ &= \inf \left\{ \int_{\Omega} R\Phi(x, u(x), \nabla u(x)) dx : u \in \mathcal{A}_{u_0} \right\}. \end{aligned} \quad (3.3)$$

We give below examples of Φ for which we obtain solutions to (3.2) for some $k \in \mathbb{N}$. This gives us an estimate of upper bounds for the energy of a solution to (3.1). The same approach for two-dimensional problems was investigated in [21].

4 The computation of $R_2\Phi$ and I_2

We start by deriving a formula for $R_1\Phi$. If

$$A = \lambda A_0 + (1 - \lambda)A_1$$

where $0 \leq \lambda \leq 1$ and $A_1 - A_0 = q \otimes r$ for $q, r : \Omega \rightarrow \mathbb{R}^3$, $|r| = 1$, then

$$A_0 = A - (1 - \lambda)q \otimes r \quad \text{and} \quad A_1 = A + \lambda q \otimes r.$$

We recall that $(q \otimes r)_{ij} = q_i r_j$. Thus, we have that

$$R_1\Phi(x, u, A) = \inf\{\Psi_1(x, u, A, \lambda, q, r) : 0 \leq \lambda \leq 1, q, r \in \mathbb{R}^3, |r| = 1\}$$

for all $x \in \Omega$, $u \in \mathbb{R}^3$, and $A \in \mathbb{R}^{3 \times 3}$, where

$$\begin{aligned} \Psi_1(x, u, A, \lambda, q, r) = & \lambda\Phi(x, u, A - (1 - \lambda)q \otimes r) \\ & + (1 - \lambda)\Phi(x, u, A + \lambda q \otimes r). \end{aligned}$$

Therefore, it follows that $I_1(u)$ for $u \in \mathcal{A}_{u_0}$ can be computed by

$$\begin{aligned} I_1(u) = \inf \left\{ \int_{\Omega} \Psi_1(x, u, \nabla u, \lambda, q, r) dx : 0 \leq \lambda \leq 1, \right. \\ \left. |r(x)| = 1 \text{ for almost all } x \in \Omega, q \in L^p(\Omega; \mathbb{R}^3) \right\}. \end{aligned}$$

We can also compute the energy minimization (3.3) using first-order laminates by

$$\begin{aligned} \inf\{I_1(u) : u \in \mathcal{A}_{u_0}\} = \inf \left\{ \int_{\Omega} \Psi_1(x, u, \nabla u, \lambda, q, r) dx : u \in \mathcal{A}_{u_0}, \right. \\ \left. 0 \leq \lambda \leq 1, |r(x)| = 1 \text{ for almost all } x \in \Omega, q \in L^p(\Omega; \mathbb{R}^3) \right\}. \end{aligned}$$

We repeat this procedure to obtain formulas for $R_2\Phi$ and I_2 . For A_0 and A_1 given as above, we consider the convex combinations

$$A_0 = \lambda_0 A_{00} + (1 - \lambda_0)A_{01} \quad \text{and} \quad A_1 = \lambda_1 A_{10} + (1 - \lambda_1)A_{11},$$

where $0 \leq \lambda_0, \lambda_1 \leq 1$ with $A_{01} - A_{00} = q_0 \otimes r_0$ and $A_{11} - A_{10} = q_1 \otimes r_1$ for $q_i, r_i \in \mathbb{R}^3$, $|r_i| = 1$, $i = 0, 1$. We thus have that

$$A = \lambda\lambda_0 A_{00} + \lambda(1 - \lambda_0)A_{01} + (1 - \lambda)\lambda_1 A_{10} + (1 - \lambda)(1 - \lambda_1)A_{11}, \quad (4.1)$$

where

$$\begin{aligned} A_{00} &= A - (1 - \lambda)q \otimes r - (1 - \lambda_0)q_0 \otimes r_0, \\ A_{01} &= A - (1 - \lambda)q \otimes r + \lambda_0 q_0 \otimes r_0, \\ A_{10} &= A + \lambda q \otimes r - (1 - \lambda_1)q_1 \otimes r_1, \\ A_{11} &= A + \lambda q \otimes r + \lambda_1 q_1 \otimes r_1. \end{aligned} \quad (4.2)$$

The representation of (4.1) as a second order laminate is illustrated in Figure 2. Roughly speaking, it represents a second order laminate with gradients oscillating among the values A_{00} , A_{01} , A_{10} , and A_{11} with volume fractions $\lambda\lambda_0$, $\lambda(1-\lambda_0)$, $(1-\lambda)\lambda_1$, and $(1-\lambda)(1-\lambda_1)$, respectively. The thickness of the black and white layers corresponds to λ , λ_0 , and λ_1 , whereas the spatial orientation of the layers is given by the normal vectors to the interfaces r , r_0 , and r_1 . The vectors q , q_0 , and q_1 denote the amplitudes of the jump of the deformation gradient over the interfaces given by the normals r , r_0 , and r_1 , respectively. The microstructures displayed below in Figures 4, 6, and 9 are also visualized in this way.

We now have that

$$R_2\Phi(x, u, A) = \inf\{\Psi_2(x, u, A, \lambda, \lambda_0, \lambda_1, q, q_0, q_1, r, r_0, r_1) : \\ 0 \leq \lambda, \lambda_0, \lambda_1 \leq 1, q, q_0, q_1, r, r_0, r_1 \in \mathbb{R}^3, |r| = |r_0| = |r_1| = 1\}$$

for $x \in \Omega$, $u \in \mathbb{R}^3$, $A \in \mathbb{R}^{3 \times 3}$, where

$$\begin{aligned} \Psi_2(x, u, A, \lambda, \lambda_0, \lambda_1, q, q_0, q_1, r, r_0, r_1) &= \lambda\lambda_0\Phi(x, u, A_{00}) \\ &+ \lambda(1-\lambda_0)\Phi(x, u, A_{01}) + (1-\lambda)\lambda_1\Phi(x, u, A_{10}) \\ &+ (1-\lambda)(1-\lambda_1)\Phi(x, u, A_{11}) \end{aligned}$$

and the A_{ij} are given by (4.2). Hence, it follows that $I_2(u)$ for $u \in \mathcal{A}_{u_0}$ can be computed by

$$I_2(u) = \inf\left\{\int_{\Omega} \Psi_2(x, u, \nabla u, \lambda, \lambda_0, \lambda_1, q, q_0, q_1, r, r_0, r_1) dx : \right. \\ \left. 0 \leq \lambda, \lambda_0, \lambda_1 \leq 1, |r(x)| = |r_0(x)| = |r_1(x)| = 1 \right. \\ \left. \text{for almost all } x \in \Omega, q, q_0, q_1 \in L^p(\Omega; \mathbb{R}^3)\right\}.$$

We can thus compute the minimization problem (3.3) by

$$\begin{aligned} &\inf\{I_2(u) : u \in \mathcal{A}_{u_0}\} \\ &= \inf\left\{\int_{\Omega} \Psi_2(x, u, \nabla u, \lambda, \lambda_0, \lambda_1, q, q_0, q_1, r, r_0, r_1) dx : u \in \mathcal{A}_{u_0}, \right. \\ &\quad \left. 0 \leq \lambda, \lambda_0, \lambda_1 \leq 1, |r(x)| = |r_0(x)| = |r_1(x)| = 1 \right. \\ &\quad \left. \text{for almost all } x \in \Omega, q, q_0, q_1 \in L^p(\Omega; \mathbb{R}^3)\right\}. \end{aligned} \tag{4.3}$$

5 The finite element discretization

We consider tetrahedral meshes $\mathcal{T}_h = \{K\}$ for Ω with the property

1. $\bar{\Omega} = \cup_{K \in \mathcal{T}_h} K$;

2. interior $K_1 \cap \text{interior } K_2 = \emptyset$ if $K_1 \neq K_2$ for $K_1, K_2 \in \mathcal{T}_h$;
3. if $S = K_1 \cap K_2 \neq \emptyset$ for $K_1 \neq K_2, K_1, K_2 \in \mathcal{T}_h$, then S is a common face, edge, or vertex of K_1 and K_2 ;
4. $\text{diam } K \leq h$ for all $K \in \mathcal{T}_h$.

We then denote the finite element spaces

$$\begin{aligned}\mathcal{U}_h &= \{v \in C(\bar{\Omega}; \mathbb{R}^3) : v \text{ is affine on each } K \in \mathcal{T}_h\} \cap \mathcal{A}_{u_0}, \\ \mathcal{L}_h &= \{\lambda : \Omega \rightarrow [0, 1] : \lambda \text{ is constant on each } K \in \mathcal{T}_h\}, \\ \mathcal{V}_h &= \{v : \Omega \rightarrow \mathbb{R}^3 : v \text{ is constant on each } K \in \mathcal{T}_h\}.\end{aligned}$$

The finite element approximation of the continuous minimization problem (4.3) is given by

$$\begin{aligned}\inf \left\{ \int_{\Omega} \Psi_2(x, u, \nabla u, \lambda, \lambda_0, \lambda_1, q, q_0, q_1, r, r_0, r_1) dx : \right. \\ \left. u \in \mathcal{U}_h, \lambda, \lambda_0, \lambda_1 \in \mathcal{L}_h, r, r_0, r_1 \in \mathcal{V}_h, q, q_0, q_1 \in \mathcal{V}_h \right\}.\end{aligned}\tag{5.1}$$

The proof of the following result on the convergence of the minimizing energy is given in Proposition 6.4.1 in [34] and [26]. Computational results for two-dimensional problems have been given in [21, 31]. In Sections 6–8, we will present computational results for three-dimensional problems.

Theorem 5.1 The problem (5.1) has a solution for any $h > 0$. Moreover,

$$\begin{aligned}\lim_{h \rightarrow 0} \min \left\{ \int_{\Omega} \Psi_2(x, u, \nabla u, \lambda, \lambda_0, \lambda_1, q, q_0, q_1, r, r_0, r_1) dx : u \in \mathcal{U}_h, \right. \\ \left. \lambda, \lambda_0, \lambda_1 \in \mathcal{L}_h, r, r_0, r_1 \in \mathcal{V}_h, q, q_0, q_1 \in \mathcal{V}_h \right\} \\ = \inf \left\{ \int_{\Omega} \Psi_2(x, u, \nabla u, \lambda, \lambda_0, \lambda_1, q, q_0, q_1, r, r_0, r_1) dx : u \in \mathcal{A}_{u_0}, \right. \\ \left. 0 \leq \lambda, \lambda_0, \lambda_1 \leq 1, r, r_0, r_1 \in L^\infty(\Omega; \mathbb{R}^3), q, q_0, q_1 \in L^p(\Omega; \mathbb{R}^3) \right\} \\ = \inf \{I(u) : u \in \mathcal{A}_{u_0}\}.\end{aligned}$$

In the computations presented in the following sections, we let $\Omega = (0, 1) \times (0, 6) \times (0, 1)$ and consider the zero displacement boundary constraint

$$u(x) = u_0(x) = x \quad \text{for } x \in \Gamma = \Gamma_1 \cup \Gamma_2,$$

where

$$\Gamma_1 = (0, 1) \times \{0\} \times (0, 1) \quad \text{and} \quad \Gamma_2 = (0, 1) \times \{6\} \times (0, 1).$$

We use a tetrahedral mesh \mathcal{T}_h obtained by subdividing the cubes in Figure 3. The mesh is symmetric with respect to the plane $x_2 = 3$.

The Fortran sequential quadratic programming routine NLPQL0 (see [37]) was used for the minimization of appropriate functions given by the discretization of the problem. Since the energy functional arising from the discretization is non-convex and NLPQL0 is designed for local optimization, we tried about 20–30 initial states for each computation in order to compute a local minimum with a sufficiently low energy. Those random states were generated by a (pseudo)random number generator. Figures 7 and 10 were obtained by successively incrementing the loading.

6 Computational experiment to show the difference between approximation by first and second order laminates

We consider the energy density

$$W_6(F) = \left| C - \begin{pmatrix} (1+\epsilon)^2 & 0 & 0 \\ 0 & \frac{1}{(1+\epsilon)^2} & 0 \\ 0 & 0 & 1 \end{pmatrix} \right|^2 \left| C - \begin{pmatrix} \frac{1}{(1+\epsilon)^2} & 0 & 0 \\ 0 & (1+\epsilon)^2 & 0 \\ 0 & 0 & 1 \end{pmatrix} \right|^2$$

for $\epsilon > 0$ where we recall that $C = F^T F$ is the right Cauchy-Green strain and that $|\cdot|$ denotes the Frobenius norm on $\mathbb{R}^{3 \times 3}$.

Here $M = 2$, the wells are defined by

$$F_1 = \begin{pmatrix} 1+\epsilon & 0 & 0 \\ 0 & \frac{1}{1+\epsilon} & 0 \\ 0 & 0 & 1 \end{pmatrix} \quad \text{and} \quad F_2 = \begin{pmatrix} \frac{1}{1+\epsilon} & 0 & 0 \\ 0 & 1+\epsilon & 0 \\ 0 & 0 & 1 \end{pmatrix},$$

and the wells are rank-one connected. We used $\epsilon = 0.1$ in the computations. We note that $W_6(\text{Id}) > 0$ where $\text{Id} \in \mathbb{R}^{3 \times 3}$ is the identity matrix. Further, it can be checked that $R_2 W_6(\text{Id}) = 0$, but $R_1 W_6(\text{Id}) > 0$. Indeed, as the problem is essentially two-dimensional we can use a procedure described in [38] to show how Id can be reached by a second-order laminate while it cannot be reached by a first-order laminate.

Thus, with load $f = 0$, we have for the identity mapping $u(x) = x$ that

$$\min_{\hat{u} \in \mathcal{A}_{u_0}} I_1(\hat{u}) > \min_{\hat{u} \in \mathcal{A}_{u_0}} I_2(\hat{u}) = I_2(u) = 0.$$

The energy of our approximate solution to the minimization of I_1 was 3×10^{-6} , while the energy of our approximate solution to the minimization of I_2 was 5×10^{-26} .

We visualize a volume fraction of the variant phase by a shade of gray on each element that is determined by a function $\gamma : \mathcal{T}_h \rightarrow [0, 1]$. Let us for notational simplicity denote $B_1 = A_{00}$, $B_2 = A_{01}$, $B_3 = A_{10}$, $B_4 := A_{11}$ and $\omega_1 = \lambda\lambda_0$, $\omega_2 = \lambda(1 - \lambda_0)$, $\omega_3 = (1 - \lambda)\lambda_1$, $\omega_4 = (1 - \lambda)(1 - \lambda_1)$. On each element $K \in \mathcal{T}_h$, we evaluate [26]

$$\gamma(K) = \sum_{l=1}^4 \omega_l^K \frac{|(B_l^K)^T B_l^K - G_1^T G_1|^2}{|(B_l^K)^T B_l^K - G_1^T G_1|^2 + |(B_l^K)^T B_l^K - G_2^T G_2|^2}, \quad (6.1)$$

where $G_1 = F_1$, $G_2 = F_2$, and \cdot^K denotes the restriction to K . We then use γ to interpolate between white (zero) and black (one).

7 Computational experiment for the cubic to tetragonal transformation

In the second numerical experiment, we utilized the Ericksen-James energy density (see [26]) which models the cubic (high temperature) to tetragonal (low temperature) transformation

$$\begin{aligned} W_7(F, \theta) = & \frac{b(\theta)}{6} \left[\left(\frac{3C_{11}}{\text{tr } C} - 1 \right)^2 + \left(\frac{3C_{22}}{\text{tr } C} - 1 \right)^2 + \left(\frac{3C_{33}}{\text{tr } C} - 1 \right)^2 \right] \\ & + \frac{c}{2} \left(\frac{3C_{11}}{\text{tr } C} - 1 \right) \left(\frac{3C_{22}}{\text{tr } C} - 1 \right) \left(\frac{3C_{33}}{\text{tr } C} - 1 \right) \\ & + \frac{d}{36} \left[\left(\frac{3C_{11}}{\text{tr } C} - 1 \right)^2 + \left(\frac{3C_{22}}{\text{tr } C} - 1 \right)^2 + \left(\frac{3C_{33}}{\text{tr } C} - 1 \right)^2 \right]^2 \\ & + e (C_{12}^2 + C_{23}^2 + C_{13}^2) + e(\text{tr } C - 3)^2, \end{aligned}$$

where $b(\theta) = 0.38 + (1.22 \times 10^{-3})(\theta - \theta_T)$, $c = -29.23$, $d = 562.13$, $e = 3.26$, $f = 5.25$, and $\text{tr } C$ denotes the trace of $C = F^T F$. These coefficients were chosen to approximately fit experimentally observed elastic moduli for the In-20.7 at% Tl alloy at the transformation temperature $\theta_T = 70^\circ \text{ C}$ [26].

The three wells ($M = 3$) are defined by F_1 , F_2 , F_3 , where

$$F_1 = \begin{pmatrix} \nu_2 & 0 & 0 \\ 0 & \nu_1 & 0 \\ 0 & 0 & \nu_1 \end{pmatrix}, \quad F_2 = \begin{pmatrix} \nu_1 & 0 & 0 \\ 0 & \nu_2 & 0 \\ 0 & 0 & \nu_1 \end{pmatrix}, \quad F_3 = \begin{pmatrix} \nu_1 & 0 & 0 \\ 0 & \nu_1 & 0 \\ 0 & 0 & \nu_2 \end{pmatrix},$$

with

$$\nu_1 = \sqrt{1 - \epsilon}, \quad \nu_2 = \sqrt{1 + 2\epsilon}, \quad \epsilon = \frac{-3b + \sqrt{9b^2 - 32a(\theta)c}}{8c}.$$

The wells are pairwise rank-one connected.

Computations for $\theta = 60^\circ$ C (so $\epsilon = 2.68 \times 10^{-2}$) and the loading $f = (-12 \times 10^{-3}, 0, 0)$ are shown in Figure 6. The top and middle figures have the perspective of Figure 3 and show the (x_1, x_2) plane, and the bottom figure shows the view from the top. The shade of gray on each element was obtained from (6.1) with $G_1 = F_1$ and $G_2 = F_2$ in the top figure and $G_1 = F_2$ and $G_2 = F_3$ for the middle and bottom figures. In addition, a microstructure corresponding to the relative volume fractions is shown for three elements of the top figure. Figure 7 uses the same graphical format to show the dependence on an increasing load parallel to $(-1, 0, 1)$.

8 The orthorhombic to monoclinic transformation

The third stored energy density that we computed models the orthorhombic to monoclinic transformation ($M = 2$) and is given by

$$W_8(F) = \left| C - \begin{pmatrix} 1 + \epsilon^2 & \epsilon & 0 \\ \epsilon & 1 & 0 \\ 0 & 0 & 1 \end{pmatrix} \right|^2 \left| C - \begin{pmatrix} 1 + \epsilon^2 & -\epsilon & 0 \\ -\epsilon & 1 & 0 \\ 0 & 0 & 1 \end{pmatrix} \right|^2 \quad (8.1)$$

where $\epsilon > 0$. We set $\epsilon = 0.1$ in our computations.

We see that the wells are given by

$$F_1 = \begin{pmatrix} 1 & 0 & 0 \\ -\epsilon & 1 & 0 \\ 0 & 0 & 1 \end{pmatrix} \quad \text{and} \quad F_2 = \begin{pmatrix} 1 & 0 & 0 \\ \epsilon & 1 & 0 \\ 0 & 0 & 1 \end{pmatrix}.$$

A similar density was used in [13, 26]. We have that $\text{rank}(F_1 - F_2) = 1$ for any $\epsilon > 0$, and therefore the wells are rank-one connected. We note that for $f = 0$ there is a unique solution $u(x) = (0.5F_1 + 0.5F_2)x = x$ for $x \in \Omega$ to the minimization problem

$$\inf_{\hat{u} \in \mathcal{A}_{u_0}} I_1(\hat{u}).$$

Figure 9 shows the deformation and microstructure computed with energy density (8.1) and load $f = (-15 \times 10^{-3}, 0, 0)$ using the shading given by (6.1) with reconstructed microstructures shown for three elements in the top plane $x_3 = 0$. Figure 10 shows the dependence on loading in the $(-1, 0, 1)$ and $(0, 0, 1)$ directions.

9 Conclusions

We have shown how the approximation to energy-minimizing deformations with microstructure for a model for martensitic crystals can be computed by using piecewise laminates. The proposed method can be derived by using an “effective” energy density, $R_2\Phi$, obtained by considering continuous, piecewise linear deformations $u(x)$ to be energy-minimizing second-order laminates on each element $K \in \mathcal{T}_h$.

The piecewise laminate finite element method gives an efficient representation of energy-minimizing deformations with microstructure. However, the piecewise laminate method requires the use of additional piecewise constant variables $0 \leq \lambda, \lambda_0, \lambda_1 \leq 1$, $q, q_0, q_1, r, r_0, r_1 \in \mathbb{R}^3$, $|r| = |r_0| = |r_1| = 1$, which make the iterative solution more challenging and less efficient. An additional challenge to the iterative solution is the “flatness” of the “effective” energy density, $R_2\Phi$, near its minimizing deformation gradients.

References

- [1] R. Abeyaratne, C. Chu, and R. James. Kinetics and hysteresis in martensitic single crystals. In *Proc. Symposium on the Mechanics of Phase Transformations and Shape Memory Alloys*. ASME, 1994.
- [2] R. Abeyaratne, C.-H. Chu, and R. D. James. Kinetics of materials with wiggly energies: theory and application to the evolution of twinning microstructures in a Cu-Al-Ni shape memory alloy. *Phil. Mag. A*, 73(2):457–497, 1996.
- [3] R. Abeyaratne and J. Knowles. On the kinetics of an austenite-martensite phase transformation induced by impact in a Cu-Al-Ni shape-memory alloy. *Acta Mater.*, 45:1671–1683, 1997.
- [4] S. Aubry, M. Fago, and M. Ortiz. A constrained sequential-lamination algorithm for the simulation of sub-grid microstructure in martensitic materials. preprint, 2002.
- [5] J. Ball and R. James. Fine phase mixtures as minimizers of energy. *Arch. Rat. Mech. Anal.*, 100:13–52, 1987.
- [6] J. Ball and R. James. Proposed experimental tests of a theory of fine microstructure and the two-well problem. *Phil. Trans. R. Soc. Lond. A*, 338:389–450, 1992.
- [7] P. Bělík, T. Brule, and M. Luskin. On the numerical modeling of deformations of pressurized martensitic thin films. *Math. Model. Numer. Anal.*, 35:525–548, 2001.

- [8] P. Bělík and M. Luskin. Stability of microstructure for tetragonal to monoclinic martensitic transformations. *Math. Model. Numer. Anal.*, 34:663–685, 2000.
- [9] P. Bělík and M. Luskin. A computational model for the indentation and phase transformation of a martensitic thin film. *J. Mech. Phys. Solids*, 50:1789–1815, 2002.
- [10] K. Bhattacharya, B. Li, and M. Luskin. The simply laminated microstructure in martensitic crystals that undergo a cubic to orthorhombic phase transformation. *Arch. Rat. Mech. Anal.*, 149:123–154, 1999.
- [11] C. Carstensen and P. Plecháč. Numerical solution of the scalar double-well problem allowing microstructure. *Math. Comp.*, 66(219):997–1026, 1997.
- [12] C. Carstensen and P. Plecháč. Numerical analysis of compatible phase transitions in elastic solids. *SIAM J. Numer. Anal.*, 37:2061–2081, 2000.
- [13] M. Chipot, C. Collins, and D. Kinderlehrer. Numerical analysis of oscillations in multiple well problems. *Numer. Math.*, 70:259–282, 1995.
- [14] C. Collins. Convergence of a reduced integration method for computing microstructures. *SIAM J. Numer. Anal.*, 35:1271–1298, 1998.
- [15] C. Collins and M. Luskin. The computation of the austenitic-martensitic phase transition. In M. Rascle, D. Serre, and M. Slemrod, editors, *Partial Differential Equations and Continuum Models of Phase Transitions*, pages 34–50, New York, 1989. Springer-Verlag. Lecture Notes in Physics, vol. 344.
- [16] B. Dacorogna. *Direct methods in the calculus of variations*. Springer-Verlag, Berlin, 1989.
- [17] G. Dolzmann. Numerical computation of rank-one convex envelopes. *SIAM J. Numer. Anal.*, 36(5):1621–1635, 1999.
- [18] Y. Efendiev and M. Luskin. Stability of microstructures for some martensitic transformations. *Math. Comput. Modelling*, 34:1289–1305, 2000.
- [19] M. Gobbert and A. Prohl. A discontinuous finite element method for solving a multiwell problem. *SIAM J. Num. Anal.*, 37:246–268, 1999.
- [20] R. Kohn and G. Strang. Optimal design and relaxation of variational problems I, II, and III. *Comm. Pure Appl. Math.*, 39:113–137, 139–182, and 353–377, 1986.

- [21] M. Kružík. Numerical approach to double well problems. *SIAM J. Numer. Anal.*, 35(5):1833–1849, 1998.
- [22] M. Kružík and A. Prohl. Young measure approximation in micromagnetics. *Numer. Math.*, 90:291–307, 2001.
- [23] B. Li and M. Luskin. Finite element analysis of microstructure for the cubic to tetragonal transformation. *SIAM J. Numer. Anal.*, 35:376–392, 1998.
- [24] Z. Li. Simultaneous numerical approximation of microstructures and relaxed minimizers. *Numer. Math.*, 78:21–38, 1997.
- [25] Z. Li. Finite order rank-one convex envelopes and computation of microstructures with laminates in laminates. *BIT*, 40:745–761, 2000.
- [26] M. Luskin. On the computation of crystalline microstructure. *Acta Numerica*, 5:191–258, 1996.
- [27] M. Luskin. Approximation of a laminated microstructure for a rotationally invariant, double well energy density. *Numer. Math.*, 75:205–221, 1997.
- [28] M. Luskin. Computational modeling of microstructure. In *Proceedings of the International Congress of Mathematicians, Beijing, 2002*.
- [29] M. Luskin and L. Ma. Analysis of the finite element approximation of microstructure in micromagnetics. *SIAM J. Numer. Anal.*, 29:320–331, 1992.
- [30] A. Mielke, F. Theil, and V. Levitas. A variational formulation of rate-independent phase transformations using an extremum principle. *Arch. Rat. Mech. Anal.*, 163:137–177, 2002.
- [31] R. A. Nicolaides and N. Walkington. Computation of microstructure utilizing Young measure representations. *J. Intelligent Material Systems and Structures*, 4:457–462, 1993.
- [32] P. Pedregal. Numerical approximation of parametrized measures. *Num. Funct. Anal. Opt.*, pages 1049–1066, 1995.
- [33] P. Pedregal. On the numerical analysis of non-convex variational problems. *Numer. Math.*, 74(3):325–336, 1996.
- [34] T. Roubíček. A note about relaxation of vectorial variational problems. In C. Bandle, et. al., editor, *Calculus of variations, applications and computations*, pages 208–214. Longman, 1995. Pitman research notes in mathematical sciences, vol. 326.

Figure 1: A visualization of W along the line between two rank-one connected deformation gradients.

Figure 2: Illustration of a second order laminate corresponding to (4.1).

- [35] T. Roubíček. Dissipative evolution of microstructure in shape memory alloys. In H.-J. Bungartz, R. W. Hoppe, and C. Zenger, editors, *Lectures on Applied Mathematics*, pages 45–63. Springer-Verlag, 2000.
- [36] T. Roubíček. Evolution model for martensitic phase transformation in shape-memory alloys. *Interfaces Free Bound.*, 4:111–136, 2002.
- [37] K. Schittkowski. NLPQL: A fortran subroutine solving constrained nonlinear programming problems. *Ann. Oper Res.*, 5:485–500, 1985.
- [38] V. Šverák. On the problem of two wells. In D. Kinderlehrer, R. James, M. Luskin, and J. Ericksen, editors, *Microstructure and Phase Transition*, pages 183–189. Springer, 1993. IMA Vol. Appl. Math. 54.

Figure 3: The reference domain Ω .

Figure 4: The computed solution with the energy density W_6 of Section 6 and load $f = 0$. The microstructure obtained from using second-order lamination is shown on the left and the microstructure obtained from using first-order lamination is shown for the same element on the right. The left half of the crystal domain is shown.

Figure 5: The reference configuration and the three variants of the martensitic phase for the cubic to tetragonal transformation described in Section 7.

Figure 6: The computed solution for the Ericksen-James energy density W_7 of Section 7 and load $f = (-12 \times 10^{-3}, 0, 0)$. The shade of gray on each element was obtained by (6.1) with $G_1 = F_1$ and $G_2 = F_2$ for the top figure (with the corresponding gray scale given by the bar in the upper right position) and $G_1 = F_2$ and $G_2 = F_3$ for the middle and bottom figures (with the corresponding gray scale given by the bar in the lower right position).

Figure 7: The computed solution for the Ericksen-James energy density W_7 of Section 7 with load $f = (-6 \times 10^{-3}s, 0, 6 \times 10^{-3}s)$ for $s \in \{2.5, 4.5, 6.5, 8.5, 10.5\}$. The shade of gray on each element was obtained by (6.1) with $G_1 = F_1$ and $G_2 = F_2$ for the top figure in each group (with the corresponding gray scale given by the top bar in the lower right pair of bars) and $G_1 = F_2$ and $G_2 = F_3$ for the middle and bottom figures in each group (with the corresponding gray scale given by the bottom bar in the lower right pair of bars).

Figure 8: The reference configuration and the two variants of the martensitic phase for the orthorhombic to monoclinic transformation described in Section 8.

Figure 9: The computed solution for the energy density W_8 and load $f = (-15 \times 10^{-3}, 0, 0)$. The shade of gray on each element was obtained by (6.1) with $G_1 = F_1$ and $G_2 = F_2$ (with the corresponding gray scale given by the bar in the right position).

Figure 10: The computed solution with the energy density W_8 and load $f = (-5 \times 10^{-3}s, 0, 5 \times 10^{-3}s)$ (left) and $f = (0, 0, 7 \times 10^{-3}s)$ (right) for $s \in \{1, 2, 3, 4, 5\}$. The shade of gray on each element was obtained by (6.1) with $G_1 = F_1$ and $G_2 = F_2$.

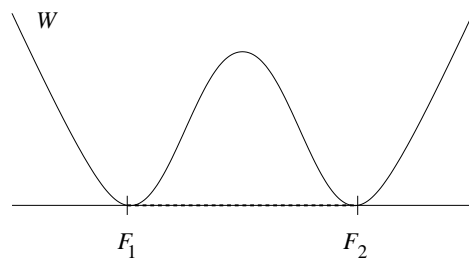


Figure 1

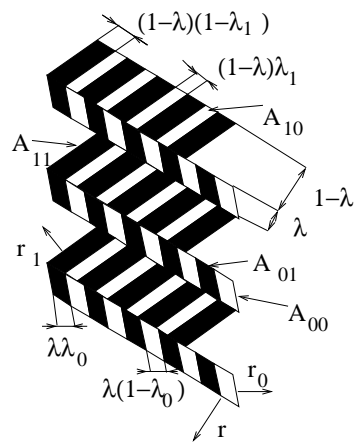


Figure 2

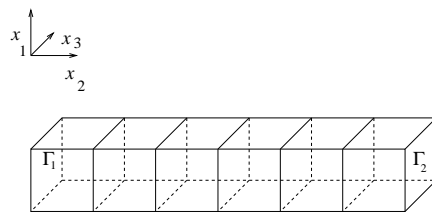


Figure 3

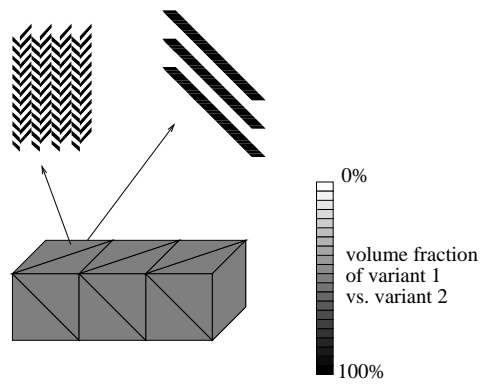


Figure 4

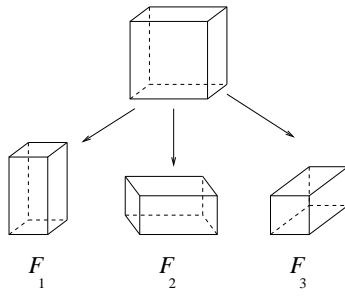


Figure 5

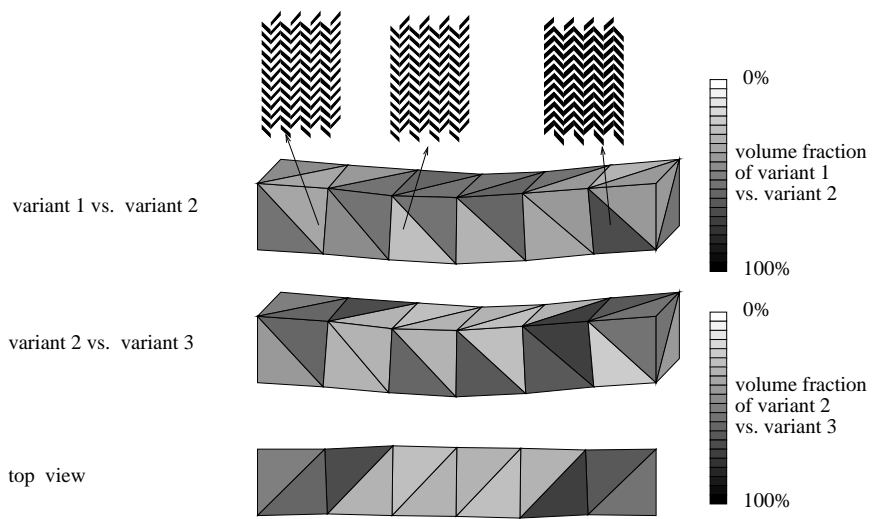


Figure 6

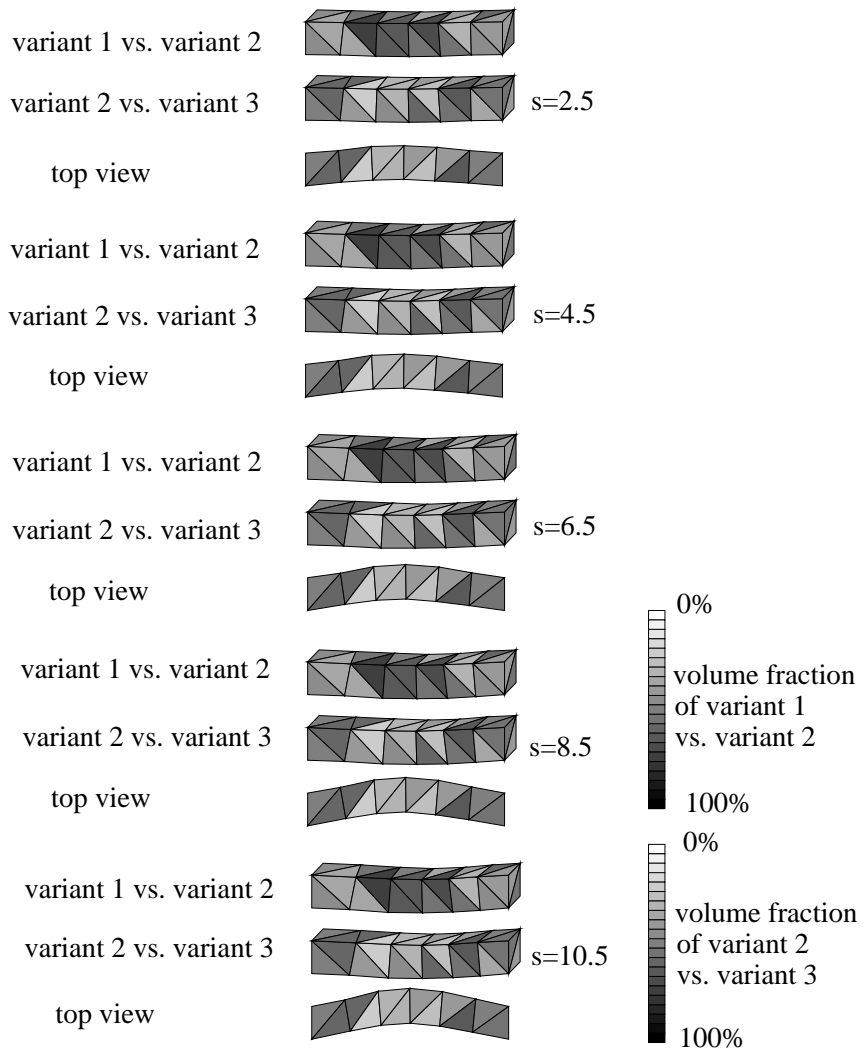


Figure 7

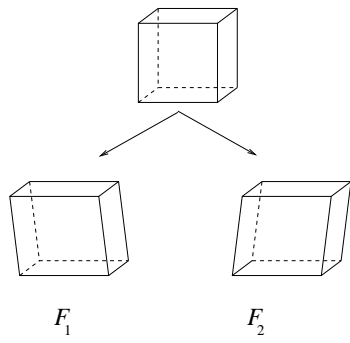


Figure 8

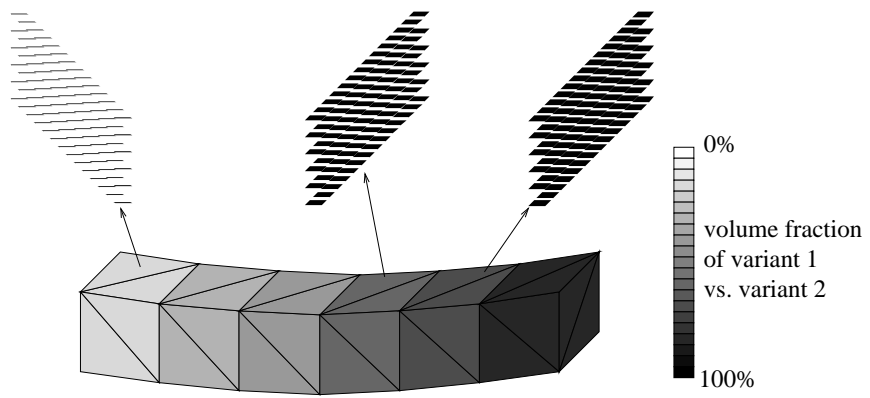


Figure 9

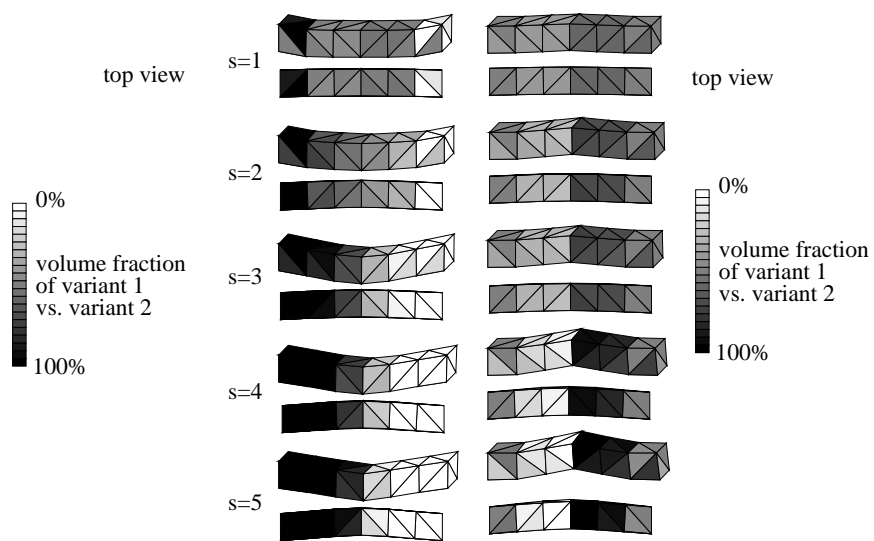


Figure 10